







DRAFT VERSION MARCH 20, 2025

Typeset using L^AT_EX preprint style in AASTeX631

Simultaneous multi-wavelength observations of the repeating fast radio burst FRB 20190520B with Swift and FAST

ZHEN YAN ¹ WENFEI YU ¹ KIM L. PAGE ² JIE LIN,^{3,4} DI LI,^{5,6,7} CHENHUI NIU,^{8,9}
CASEY LAW,^{10,11} BING ZHANG ^{12,13} SHAMI CHATTERJEE,¹⁴ XIAN ZHANG ^{1,15} AND
RESHMA ANNA-THOMAS ^{16,17}

¹Shanghai Astronomical Observatory, Chinese Academy of Sciences, 80 Nandan Road, Shanghai 200030, China

²School of Physics & Astronomy, University of Leicester, LE1 7RH, UK

³CAS Key laboratory for Research in Galaxies and Cosmology, Department of Astronomy, University of Science and Technology of China, Hefei 230026, China

⁴School of Astronomy and Space Sciences, University of Science and Technology of China, Hefei 230026, China

⁵Department of Astronomy, Tsinghua University, Beijing 100084, China

⁶National Astronomical Observatories, Chinese Academy of Sciences, A20 Datun Road, Chaoyang District, Beijing 100101, China

⁷Zhejiang Lab, Hangzhou, Zhejiang 311121, People's Republic of China

⁸National Astronomical Observatories, Chinese Academy of Sciences, Beijing 100012, China

⁹Institute of Astrophysics, Central China Normal University, Wuhan 430079, China

¹⁰Cahill Center for Astronomy and Astrophysics, MC 249-17 California Institute of Technology, Pasadena, CA 91125, USA

¹¹Owens Valley Radio Observatory, California Institute of Technology, 100 Leighton Lane, Big Pine, CA, 93513, USA

¹²The Nevada Center for Astrophysics, University of Nevada, Las Vegas, Las Vegas, NV 89154, USA

¹³Department of Physics and Astronomy, University of Nevada, Las Vegas, Las Vegas, NV 89154, USA

¹⁴Cornell Center for Astrophysics and Planetary Science, and Department of Astronomy, Cornell University, Ithaca, NY, USA.

¹⁵University of Chinese Academy of Sciences, 19A Yuquanlu, Beijing 100049, China

¹⁶West Virginia University, Department of Physics and Astronomy, P.O. Box 6315, Morgantown, WV, USA

¹⁷Center for Gravitational Waves and Cosmology, West Virginia University, Chestnut Ridge Research Building, Morgantown, WV, USA

ABSTRACT

Among several dozen known repeating Fast radio bursts (FRBs), those precisely localized offer the best opportunities to explore their multi-wavelength counterparts, which are key to uncovering their origins. Here we report our X-ray, ultraviolet (UV), and optical observations with the *Swift* satellite of the repeating FRB 20190520B, in coordination with simultaneous radio observations with the Five-hundred-meter Aperture Spherical radio Telescope (FAST). Our aim was to detect potentially associated multi-wavelength bursts and identify any persistent multi-wavelength counterpart to the associated persistent radio source (PRS). While a total of 10 radio bursts were detected by FAST during the *Swift* observations, we detected no X-ray, UV, or optical bursts

Corresponding author: Wenfei Yu

wenfei@shao.ac.cn

in accompany with the radio bursts. We obtained the energy upper limits (3σ) on any multi-wavelength bursts as follows: 5.03×10^{47} erg in the hard X-ray band (15–150 keV), 7.98×10^{45} erg in the soft X-ray band (0.3–10 keV), and 4.51×10^{44} erg in the U band (3465Å), respectively. The energy ratio between soft X-ray (0.3–10 keV) and radio emission of the bursts is constrained as $< 6 \times 10^7$, and the ratio between optical (U band) and radio as $< 1.19 \times 10^6$. We detect no multi-wavelength counterpart to the PRS. The 3σ luminosity upper limits are 1.04×10^{47} (15–150 keV), 8.81×10^{42} (0.3–10 keV), 9.26×10^{42} (UVW1), and 2.54×10^{42} erg s $^{-1}$ (U), respectively. We show that the PRS is much more radio loud than representative pulsar wind nebulae, supernova remnants, extended jets of Galactic X-ray binaries, and ultraluminous X-ray sources, suggestive of boosted radio emission of the PRS.

1. INTRODUCTION

Fast radio bursts (FRBs) are radio bursts with a typical duration on the millisecond timescale. They have been observed with dispersion measure (DM) larger than that of the Galactic values, indicating their cosmological origins (see [Zhang 2023](#), for a review). Due to their short duration, localization of the FRBs has been challenging in the radio band, with only tens of FRBs precisely localized among a sample of around 1000 so far. The search for potential persistent and transient multi-wavelength counterparts, through ground or space observations, largely depends on their precise localization to the arc-second scale or better.

The observed FRB population includes repeating FRBs and non-repeating FRBs. The relationship between these two potential sub-categories and whether they originate from distinct sources remains undetermined. Repeating FRBs, particularly those in their active phase, are prime targets to perform multi-wavelength campaigns aimed at identifying potential burst counterparts across different wavelengths on timescales as short as milliseconds. Despite extensive efforts to search for multi-wavelength counterparts in the optical, X-ray and gamma ray bands in the past (e.g. [Scholz et al. 2017](#); [Sun et al. 2019](#); [Guidorzi et al. 2020a,b](#); [Pilia et al. 2020](#); [Tavani et al. 2020](#); [Laha et al. 2022](#); [Hiramatsu et al. 2023](#); [Principe et al. 2023](#); [Trudu et al. 2023](#); [Kilpatrick et al. 2024](#)), no positive detection had been made by the time when this paper was submitted.

Among the entire sample, FRB 20121102A is the first known FRB associated with a persistent radio source (PRS) ([Chatterjee et al. 2017](#)). Searches for potential multi-wavelength counterparts of the PRS has also yielded non-detections (e.g. [Chatterjee et al. 2017](#); [Scholz et al. 2017](#); [Chen et al. 2023](#); [Eftekhari et al. 2023](#)). The observations of the host galaxy of FRB 20121102A were used to set an upper limit on the optical and infrared counterparts of the PRS ([Bassa et al. 2017](#); [Chatterjee et al. 2017](#); [Tendulkar et al. 2017](#)).

The Five-hundred-meter Aperture Spherical radio Telescope (FAST; [Nan et al. 2011](#)) is equipped with 19-beams receiver to enlarge its field of view in L-band. FRB 20190520B was discovered from archived data in Commensal Radio Astronomy FAST Survey (CRAFTS; [Li et al. 2018](#); [Li et al. 2019](#)). It is an active repeating FRB source from which four bursts were detected in the drift scan survey in 2019. Three bursts were detected in the same beam during the drift scan, and the fourth was followed up in another beam. By checking the beam pointings at the time of events, FAST observations localized the FRB to a position accurate to a few arc-minutes. Through the VLA DDT/20A-557 program, we localized the bursts to the sub-arcsecond accuracy with the discovery of

a PRS in spatial association with the bursts and determine the redshift of the FRB 20190520B as 0.241 after the identification of its host galaxy (Niu et al. 2022). With the refined burst and PRS positions, we are able to search for multi-wavelength counterparts for the radio bursts and the PRS, respectively.

FRB 20190520B has been persistently active ever since its discovery and remains the only such repeater without any extended dormant periods (e.g. longer than a few days). This makes it an ideal target for follow-up with multi-band observations. It also produced plenty of bursts with a high signal-to-noise ratio ($S/N \sim$ a few tens) as seen with FAST in our campaign. Therefore, multi-wavelength observations conducted simultaneously or quasi-simultaneously with FAST observations could yield valuable upper limits or even potential detection of multi-wavelength bursts in temporal association with these radio bursts. Such results of multi-wavelength bursts would provide crucial information about the central engine of the FRB 20190520B (e.g. Nicastro et al. 2021; Zhang 2023), thereby revealing the nature of the repeating FRBs or the FRBs as a whole.

On the other hand, the nature of the PRS and its relation to the FRB bursting source remain unclear. The multi-wavelength properties of the PRS can provide a critical and complementary test for current FRB models due to its physical and positional association with the FRB source. As one of the known FRBs associated with a PRS, detecting a potential multi-wavelength counterpart of the PRS would be a major step towards the understanding of the origin of PRS and its physical relation to the FRB source.

The *Swift* mission can be flexibly scheduled and is able to quickly respond for target-of-opportunity (ToO) observations of transient events in hard X-ray, soft X-ray, and ultraviolet (UV)/optical bands (Gehrels et al. 2004). It consists of three major instruments: the Burst Alert Telescope (BAT), the X-Ray Telescope (XRT) and the Ultraviolet/Optical Telescope (UVOT). BAT covers the hard X-ray band ($\sim 15\text{--}150$ keV) and is capable of searching for any bright hard X-ray bursts or persistent sources if the target is in its large field-of-view. XRT is a focusing X-ray telescope that covers the soft X-ray band (0.3–10 keV). It has a time resolution of 2.51 seconds in photon-counting (PC) mode and 1.8 milliseconds in windowed-timing (WT) mode, allowing it to detect potential soft X-ray bursts or a persistent X-ray counterpart. UVOT is equipped with six filters in the UV/optical band and can collect event mode data with high time resolution (~ 12 milliseconds), enabling it to detect potential UV/optical bursts and also any persistent counterparts.

Here we report our simultaneous *Swift* and FAST observations of the FRB 20190520B performed in May and August of 2020. The PRS position of FRB 20190520B is coincident with the burst within the uncertainty at coordinates 16:02:04.266, -11:17:17.33, obtained from the VLA observation (Niu et al. 2022; Zhang et al. 2023). We used these coordinates in the following *Swift* data analysis to search for potential burst counterpart on timescale of seconds to milliseconds, and to search for the PRS counterpart with long exposures lasting thousands to tens of thousands of seconds.

2. OBSERVATIONS

We requested two sets of simultaneous *Swift* and FAST Target-of-Opportunity (ToO) observations of FRB 20190520B in May and August of 2020. The first *Swift*/FAST campaign in May 2020 aimed to detect potential X-ray bursts in both soft X-ray band (XRT) and hard X-ray band (BAT) in association with the radio bursts detected by a single FAST observation. Additionally, we performed an initial investigation of the field in UV wavelengths using *Swift*/UVOT and searched for potential UV bursts. The second *Swift*/FAST campaign in August 2020 was primarily aimed at fast optical

photometric observations performed simultaneously with FAST observations after our target was confirmed active in the radio band and a sub-arcsecond localization was achieved by the VLA.

The corresponding FAST observations were all conducted in tracking mode. The May 2020 campaign targeted the position determined by previous FAST drift scan and tracking observations. The August 2020 campaign pointed at the position obtained by our preliminary localizations of the radio bursts and the PRS measured with the VLA at the time of the observations.

2.1. FAST observations

The FAST observations coeval with the *Swift* observations were obtained through Director’s Discretionary Time (DDT2020_3) and the FAST key science project. Based on the initial coarse localization of FRB 20190520B from the analysis of partially overlapping drift scans as part of the CRAFTS design (Li et al. 2018), FAST observations of FRB 20190520B started on April 25, 2020, during which multiple bursts were successfully detected. On May 22, in the FAST observation conducted jointly with *Swift*, 13 bursts were observed, further indicating that this source was active.

In late July, after our VLA DDT program had successfully localized the bursts to arc-second accuracy, we requested an additional simultaneous campaign on FRB 20190520B with *Swift* and FAST, utilizing the precise localization. This campaign lasted from August 4 to August 16, 2020, during which a total of 7 *Swift* observations were carried out, one every two days (Table 1). During this period, 6 FAST observations were performed. FAST could track FRB 20190520B for ~ 1.7 hours each day due to the constraint by the observation window. In total, 40 radio bursts were detected at L band by FAST during this campaign (Niu et al. 2022), 10 of which are covered by the time windows of the *Swift* observations (Table 3).

2.2. Swift observations

We requested a single *Swift* ToO observation on 2020 May 22 and seven additional ones during the first half of 2020 August Table 1, which were coordinated with FAST observations. These observations allowed us to search for potential simultaneous optical bursts down to a timescale as short as ~ 12 ms (event mode of U band), and for potential simultaneous X-ray bursts down to a timescale of 2.51 seconds (PC mode of XRT). Since no BAT event data were taken during those targeted *Swift* observations, we retrieved the BAT event data with exposures longer than 100 seconds and within 30° of the FRB 20190520B position during the period of the FAST observations (MJD 58962–59112; Niu et al. 2022) to search for potential hard X-ray counterpart of the radio bursts. The observation information is listed in Table 2.

In the *Swift* archive, we identified a previous XRT observation from 2016 that covered the field of FRB 20190520B. This observation, triggered by a non-GRB event, was pointed approximately 5 arc-minutes away from FRB 20190520B. We have included this observation in our analysis to constrain the X-ray counterpart of the PRS (see Table 1). We utilize all the *Swift* observations in Table 1 to the search for potential PRS counterparts in hard X-ray (survey data of BAT), soft X-ray (XRT), optical (U band) and ultraviolet (UVW1 band).

3. DATA ANALYSIS AND RESULTS

3.1. upper limits on the persistent emission

Table 1. The information of the *Swift* observations and the upper limits

obsID	start time (UTC)	exposure (s)	filter	AB Mag	Flux (μ jy)	XRT rate (10^{-3} c/s)
00034397001	2016-02-27 22:58:04	744	U	> 21.73	< 7.50	< 12.39
00013503001	2020-05-22 17:09:35	1396	UVW1	> 22.24	< 4.54	< 6.31
00013503002	2020-08-04 11:29:35	1378	U	> 22.22	< 4.77	< 6.27
00013503003	2020-08-06 11:12:35	1669	U	> 22.33	< 4.33	< 5.22
00013503004	2020-08-08 10:57:34	1558	U	> 22.27	< 4.56	< 7.70
00013503005	2020-08-10 10:53:35	1411	U	> 22.15	< 5.10	< 6.37
00013503006	2020-08-12 10:39:35	1557	U	> 22.26	< 4.60	< 6.17
00013503007	2020-08-14 10:28:36	1398	U	> 22.19	< 4.89	< 5.80
00013503008	2020-08-16 11:42:35	1368	U	> 22.13	< 5.19	< 6.51

Note: All of them correspond to 3σ upper limits.

Assuming a power law X-ray spectrum with a photon index of 2 and a Galactic hydrogen column density of $2.6 \times 10^{21} \text{ cm}^{-2}$, an XRT rate of 1 counts s^{-1} corresponds to unabsorbed X-ray flux of $5.77 \times 10^{-11} \text{ erg cm}^{-2} \text{ s}^{-1}$ in the 0.3–10 keV band. Similarly, a BAT rate of $1 \text{ counts s}^{-1} \text{ cm}^{-2}$ corresponds to unabsorbed X-ray flux of $8.33 \times 10^{-8} \text{ erg cm}^{-2} \text{ s}^{-1}$ in the 15–150 keV band, according to the conversion from WebPIMMS². These fluxes correspond to $9.94 \times 10^{45} \text{ erg s}^{-1}$ (0.3–10 keV) and $1.48 \times 10^{49} \text{ erg s}^{-1}$ (15–150 keV) for the distance of 1218 Mpc of FRB 20190520B (Niu et al. 2022). We can use this conversion to roughly estimate the X-ray flux in the following analysis.

For each Swift/XRT observation, we determined the 3σ upper limit (see Table 1) using the online Swift/XRT products generator³ (Evans et al. 2007), as there were no positive detection in individual observation at the PRS position of FRB 20190520B. We then stacked all the nine XRT observations and obtained the X-ray count rate upper limit of $8.6 \times 10^{-4} \text{ c/s}$ at the PRS position. Using the aforementioned flux conversion, the upper limit on the 0.3–10 keV X-ray flux of the potential counterpart of the PRS is $4.96 \times 10^{-14} \text{ erg cm}^{-2} \text{ s}^{-1}$, corresponding to an X-ray luminosity of $8.81 \times 10^{42} \text{ erg s}^{-1}$.

For each *Swift*/UVOT observation, photometric analysis was performed using the task `uvotsource` with a recommended aperture radius of $3''$ ⁴. All the photometric results of each observation are listed in Table 1. None of the observations yielded a positive detection of the persistent source at the PRS position of the FRB 20190520B. To determine the limiting magnitude of the optical counterpart of the PRS, we stacked the images from the eight observations performed with the U filter (see Table 1). We achieved a 3σ upper limit as 23.36 (AB magnitude) in the *U*-band for the persistent source at the FRB 20190520B position, corresponding to a luminosity of $2.54 \times 10^{42} \text{ erg s}^{-1}$. There was only one observation performed with the UVW1 filter; the upper limit of the PRS is 22.25 (AB magnitude), corresponding to $9.26 \times 10^{42} \text{ erg s}^{-1}$.

The BAT survey data were processed with the `batsurvey` script. Subsequently, we employed `batcelldetect` to determine the SNR at the PRS position in BAT sky images. The highest SNR obtained was 2.3σ , which is significantly below the recommended detection threshold of 5σ . The

¹ <https://www.swift.ac.uk/analysis/nhtot/index.php>

² <https://heasarc.gsfc.nasa.gov/Tools/w3pimmshelp.html>

³ https://www.swift.ac.uk/user_objects/

⁴ https://swift.gsfc.nasa.gov/analysis/threads/uvot_thread_aperture.html

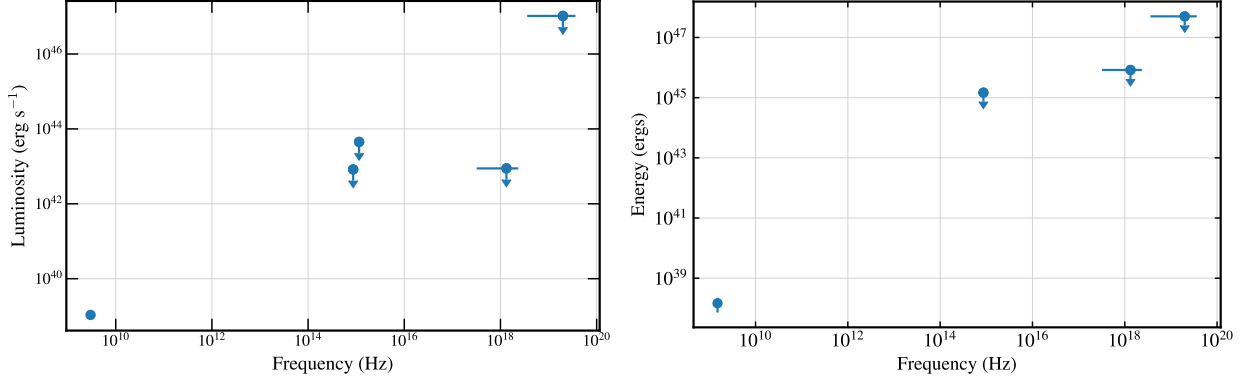


Figure 1. Left: The broad band SED of the PRS of the FRB 20190520B. The radio luminosity is taken from Niu et al. (2022); the upper limits in wavelengths other than the radio band are obtained in this work. Right: The broad band SED of the burst emission of FRB 20190520B. The radio energy is averaged over the burst sample listed in Niu et al. (2022); the upper limits in wavelengths other than the radio band are constrained and obtained in this work.

upper limit of the hard X-ray counterpart of the PRS can be estimated from background level. The 3σ upper limit is about $0.007 \text{ counts s}^{-1} \text{ cm}^{-2}$ (15–150 keV) with exposure time 1677 seconds. This corresponds to the X-ray flux of $5.83 \times 10^{-10} \text{ erg s}^{-1} \text{ cm}^{-2}$, assuming a power-law spectrum with index of 2, and an X-ray luminosity of $1.04 \times 10^{47} \text{ erg s}^{-1}$.

We then plotted the broad band spectral energy distribution (SED, Figure 1). The radio flux of PRS is used as $202 \pm 8 \mu\text{Jy}$ (Niu et al. 2022). For the calculation of U and UVW1 fluxes, we applied an extinction of $E(B - V) = 0.26$ (Niu et al. 2022).

3.2. upper limits on the burst emission

We also estimate the upper limits on the simultaneous X-ray and optical fluxes of the radio burst detected by FAST. The dispersion delay corresponding to infinite frequency is calculated by using the DM in Table 3. Subsequently, we correct the burst time to search for the potential simultaneous bursts at X-ray and optical bands.

Since no BAT event data were obtained in the observations listed in Table 1, we used the observations listed in Table 2 to search for potential hard X-ray bursts, as FRB 20190520B remained active during this period. We extracted the light curves (15–150 keV) at the burst position using the tool `batbinevt` with a time resolution of 10 ms. This time resolution was chosen because it is comparable to the typical duration of the radio bursts observed with FAST and meets the photon statistics required for the burst search. Subsequently, we searched for coincident X-ray bursts in the 15–150 keV band based on the dispersion delay corrected burst arrival times. Unfortunately, none of the radio bursts detected by FAST were covered by the *Swift*/BAT event data within a span of 1000 seconds.

We then used the standard deviation of the count rate on 10 ms timescale to estimate the 3σ upper limit on potential X-ray bursts as $3.40 \text{ counts s}^{-1} \text{ cm}^{-2}$. This corresponds to an X-ray flux (15–150 keV) of $2.83 \times 10^{-7} \text{ erg s}^{-1} \text{ cm}^{-2}$, assuming a power law index of 2, and a luminosity of $5.03 \times 10^{49} \text{ erg s}^{-1}$. The burst energy can be estimated according to $L \times \delta t$, where L is the upper limit of the luminosity and δt is the time resolution. The upper limit of the luminosity in the non-detection case is determined by the instrumental sensitivity, which depends on the chosen time resolution.

Therefore, we opted to use energy as the upper limit measurement of the burst emission rather than luminosity, as it is independent of the choice of a certain time resolution, and ensures a homogeneous comparison across the outcomes of instruments with different time resolutions. The upper limit of the burst energy in the 15–150 keV band is $\sim 5.03 \times 10^{47}$ erg.

The *Swift*/XRT observations were performed in the PC mode. In order to estimate the soft X-ray upper limit for each radio burst detected by FAST, we used the online tool (Evans et al. 2007) to generate the light curve of each observation with a time resolution of 2.51 seconds. A total of 10 radio bursts were simultaneously covered by the *Swift*/XRT observations; with upper limits on the burst emission ranging from 3.20 to 3.63 c/s. The corresponding upper limits on the X-ray luminosity and energy are roughly estimated as $(3.28\text{--}3.72) \times 10^{46}$ erg s $^{-1}$, and $(8.22\text{--}9.34) \times 10^{46}$ erg. We also searched for potential X-ray burst within the 100 s interval around each radio burst. No positive detection is archived, and the upper limit remain within the aforementioned range. It is worth noting that only two photons detected within the PSF (18'') of the burst position during the total exposure of ~ 12400 seconds.

We then extracted available *Swift*/XRT images coincident with the radio burst using `xselect`, with a time resolution of 2.51 seconds. Corresponding exposure maps are also produced. We then stacked all the 10 XRT sky images and exposure maps, and obtained a 3σ upper limit as 0.32 counts s $^{-1}$ using the tool `sosta`. This count rate corresponds to an upper limit on X-ray luminosity of 3.18×10^{45} erg s $^{-1}$, and an upper limit on X-ray energy of 7.98×10^{45} erg.

We also notice that the DM is very large ~ 1200 pc cm $^{-3}$ for FRB 20190520B. According to the correlation between the DM and X-ray column density in He et al. (2013), the corresponding column density of FRB 20190520B is about 3.6×10^{22} cm $^{-2}$. The unabsorbed X-ray flux observed by the XRT in the 0.3–10 keV band is about four times larger than previous estimations, which were based solely on Galactic column density in the source's direction. However, the unabsorbed X-ray flux as seen with BAT in the 15–150 keV range remains unchanged. The origin of DM is still uncertain for these bursts (Niu et al. 2022), and local contributions are likely significant (Lee et al. 2023). For the purposes of order-of-magnitude estimation, we will continue to use the X-ray flux upper limits derived from the Galactic column density in the followings.

One of the aims of the August 2020 campaign was to perform fast photometry in the optical band to search for the optical burst counterparts. Seven *Swift*/UVOT observations with U filter (3465Å) were conducted in event mode. We first used `uvotscreen` to obtain the corresponding cleaned event data. The astrometry of the event data is then refined by using the method in Oates et al. (2009). We extracted *U*-band images every 100 s. The position of each photon event was corrected based on the differences obtained from cross-correlating the image with the USNO-B1 catalogue. We then used the `uvotevtlc` task to generate the corresponding light curve with a time resolution of 12 milliseconds from each event file, applying a circular source region with a radius of 3''. Consequently, the upper limits on the source flux in the time resolution of 12 milliseconds, which were simultaneous with any radio burst detected by FAST, were obtained. The upper limits on the luminosity and burst energy on the timescale of 12 ms for 9 available bursts are the same as 3.76×10^{46} erg s $^{-1}$ and 4.51×10^{44} erg. We also searched the 100s interval around each radio burst but found no positive detection. The upper limit remains the same.

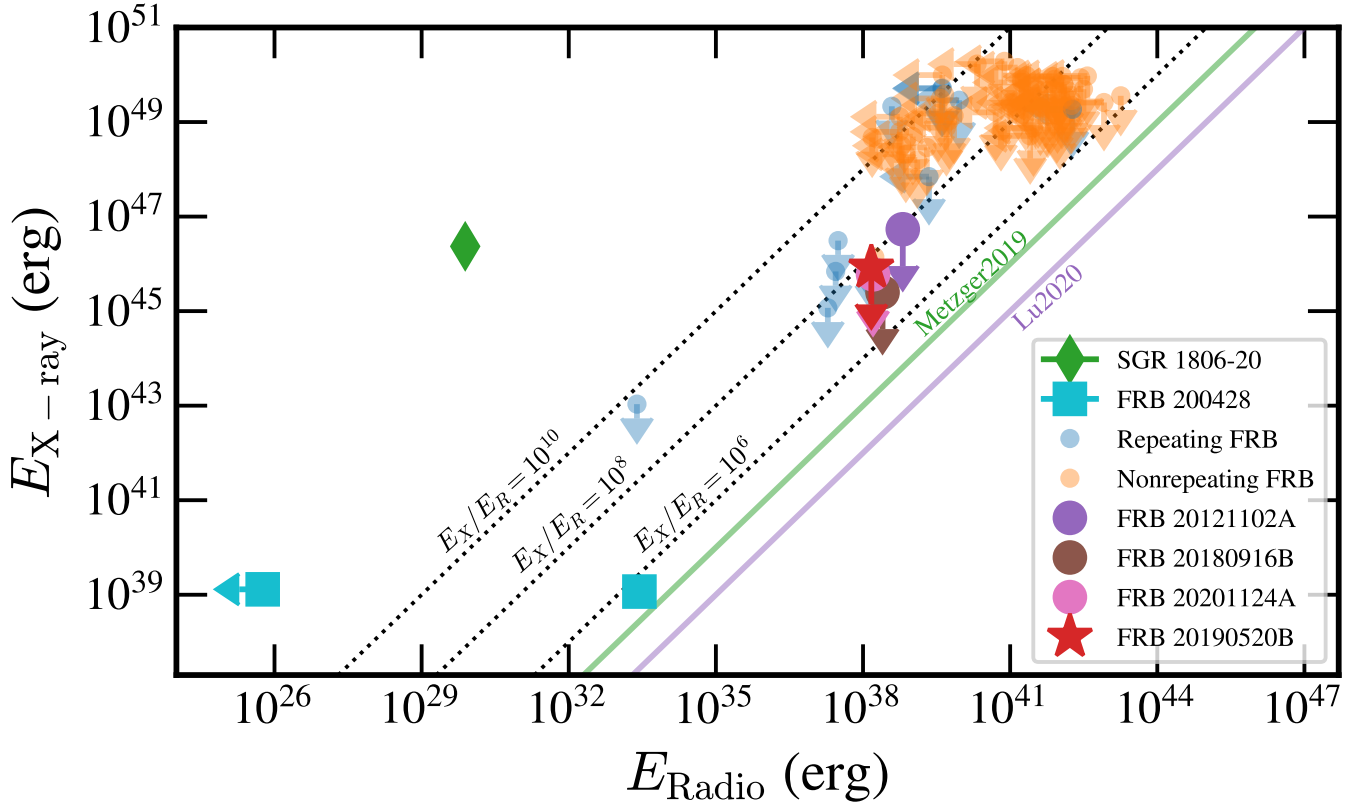


Figure 2. The relationship between X-ray and radio energy of bursts in the FRBs. The data, except for FRB 20190520B, are taken from Scholz et al. (2017); Guidorzi et al. (2020a); Laha et al. (2022). The green and purple lines are the model prediction from Metzger et al. (2019) and Lu et al. (2020), respectively. For many FRBs, the distances are constrained as upper limits, so the burst energy in both X-ray and radio bands are also upper limits.

We then use the burst energy upper limit extracted from the stacked XRT images, BAT event data and U band event data to plot the broad band SED of the burst emission in Figure 1. The average burst energy at 1.5 GHz and $E(B-V)=0.258$ from Niu et al. (2022) is adopted.

Using the average radio burst energy in Niu et al. (2022) and the X-ray burst energy upper limit from stacked XRT images, we derived the upper limit of the X-ray-to-radio energy ratio $E_X/E_R < 6 \times 10^7$.

4. DISCUSSION

Repeating FRBs offer a valuable opportunity for burst localization and the search for multi-wavelength counterparts. However, over the past few years, significant challenges have persisted in the efforts towards the detection of FRB counterparts, both from space and ground-based observations. In May and August 2020, we conducted simultaneous *Swift* pointed observations with FAST tracking observations of the actively repeating fast radio burst FRB 20190520B, the second known FRB associated with a compact PRS. Here, we report the results of multi-wavelength counterparts of both the bursts and the PRS from our *Swift* campaign. Utilizing short and long exposures from the BAT, XRT and UVOT onboard *Swift*, we placed constraints on potential multi-wavelength counterparts to the radio bursts and the PRS, based on precise localization of the source by the VLA in 2020.

4.1. Burst counterparts

In our campaign, *Swift* observations simultaneously covered 10 radio bursts detected by FAST (see Table 3). No X-ray or optical burst events were detected. We derived upper limits for the burst flux on short timescales in both the soft X-ray (0.3–10 keV, 2.51 seconds), hard X-ray (15–150 keV, 10 ms) and optical (U band, 12 ms) bands (see subsection 3.2). The current measurements are constrained by the sensitivity of the instruments at these short timescales. Since the upper limit on burst luminosity depends on the time resolution used, it is more appropriate to use the upper limit on burst energy to constrain the multi-wavelength emission.

Chen et al. (2020) estimated the ratio η , which represents the energy of FRB counterparts at various wavelengths compared to the radio wavelength, based on the non-detection from various surveys and instruments. This ratio is crucial for constraining emission models across multiple wavelengths. We derive a lower limit of the ratio $\eta = E_X/E_R \lesssim 6 \times 10^7$ and $\eta = E_U/E_R \lesssim 10^6$. Additionally, using the radio and X-ray burst energy values from an FRB sample reported by Laha et al. (2022) and Guidorzi et al. (2020a), we re-plotted the relation between E_R and E_X (Figure 2).

The upper limits on the burst fluences in the X-ray band are mainly constrained by the instrument sensitivity at short timescales. Notably, the values of upper limits for E_X tend to saturate around 10^{50} ergs. For many FRBs, the burst energy in both X-ray and radio bands are constrained as upper limits, because their distances correspond to upper limits. For comparison, we also marked the upper limits obtained for FRB 20121102A (Scholz et al. 2017), FRB 20180916B (Pilia et al. 2020; Trudu et al. 2023) and FRB 20201124A (Piro et al. 2021) in Figure 2. These FRBs have been active, with extensive multi-wavelength campaigns to search for the burst counterparts. They show comparable upper limits of $E_X/E_R \sim 10^7 - 10^8$, similar to that of FRB 20190520B.

The discovery of Galactic FRB 20200428 (Bochenek et al. 2020, SGR 1935+2151;) suggests a potential magnetar origin for FRBs, though the energy budget remains a major concern for magnetar models (Li et al. 2021). FRB 20200428 is much weaker than most FRBs, by several orders of magnitude. On the other hand, thousands of bursts from FRB 20121102A were observed within a time span of 47 days, adding up to a substantial fraction of total available magnetic energy from a magnetar (Li et al. 2021). The prolonged burst activities of FRB 20190520B poses even greater challenges for the magnetar models.

FRB emission generally fall into two categories in the magnetar-based models: those invoking emission inside the magnetosphere of the magnetar (e.g. Kumar et al. 2017; Yang & Zhang 2018; Lu et al. 2020) and those invoking relativistic shocks outside the magnetosphere (e.g. Lyubarsky 2014; Metzger et al. 2019; Beloborodov 2020). The latter predicts a relatively large E_X/E_R (Sironi et al. 2021), while the former allows for a smaller ratio (Zhang 2020). Our constraints on FRB 20190520B exceed the prediction of both models (Figure 2, see also Chen et al. 2020). More sensitive X-ray/optical telescopes are required for current FRB samples, or only very nearby extragalactic X-ray/optical bursts will be detectable if these model predictions hold.

4.2. PRS counterpart

The PRS in association with the FRB 20190520B exhibits peculiar variability, suggesting the possibility of an accreting compact object scenario (Zhang et al. 2023). Constraining the multi-wavelength counterpart is crucial for uncovering and understanding the true nature of the PRS. By stacking the XRT observations, we obtained an upper limit on the persistent flux of 8.81×10^{42} erg s⁻¹. Addition-

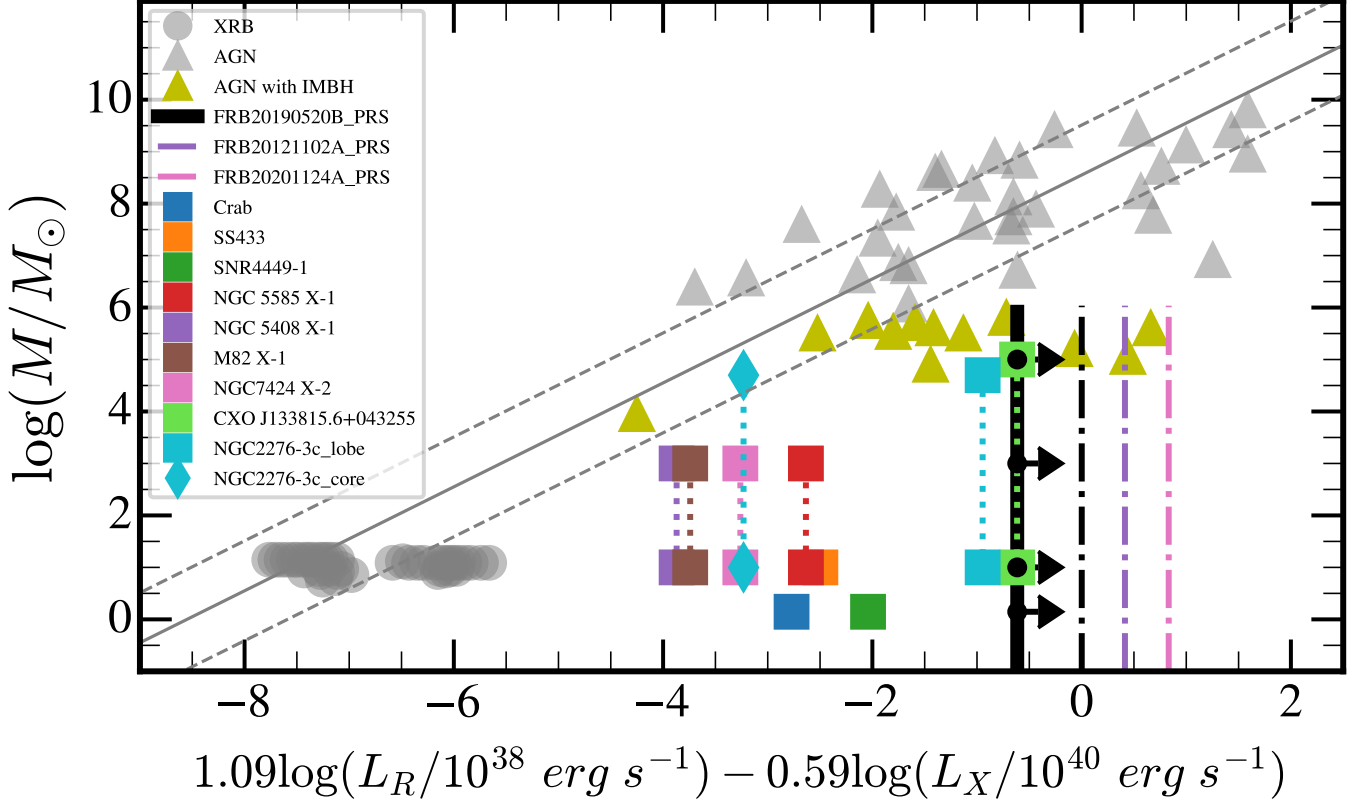


Figure 3. The gray data points, solid lines, and dashed lines represent the data for XRBs, AGNs, and best-fitting results for the fundamental plane of accretion and jet activity of different scales of BHs (Gültekin et al. 2019). Different kinds of systems are also plotted in this diagram, including PWN, SNR, XRB nebula and ULXs. The solid black line represents the lower limit of the PRS of FRB 20190520B derived in this work, and the black dots with arrows are assumed BH masses of 10^5 , 10^3 , 10 and $1.4 M_\odot$. The black dash-dotted line is the lower limit of the PRS of FRB 20190520B calculated from the X-ray constraint with *Chandra*. The purple and pink dash-dotted lines represent the lower limit of the PRSs for FRB 20121102A and FRB 20201124A.

ally, the upper limits on a potential persistent counterpart were obtained as $2.54 \times 10^{42} \text{ erg s}^{-1}$ at U band and $9.26 \times 10^{42} \text{ erg s}^{-1}$ at UVW1 band.

As the two active FRBs and the best known FRBs associated with a compact PRS, FRB 20190520B and FRB 20121102A share striking similarities in their burst environment. Both are hosted by dwarf galaxies with high star formation rates (Chatterjee et al. 2017; Niu et al. 2022). If the central engine is a magnetar, the PRS could correspond to a pulsar wind nebula (PWN) or a supernova remnant (SNR). However, the radio flux and spectra of the PRSs show variations on timescales as short as days, suggesting that a significant fraction of the instant PRS radio emission may result from accretion onto a compact object (Zhang et al. 2023; Rhodes et al. 2023). Additionally, their extremely large and variable rotation measures imply that they exist within dynamic, highly magnetized environments (Michilli et al. 2018; Anna-Thomas et al. 2023).

On the other hand, it has been suggested that binary systems may lie behind FRB sources (e.g. Chen et al. 2022). The periodic activity of FRB 20121102A (Rajwade et al. 2020) and the sign reversal of the rotation measure of FRB 20190520B (Anna-Thomas et al. 2023) have led to models

proposing a binary system. Sridhar & Metzger (2022) have put forward a scenario where a nebula surrounding a hyper-accretion X-ray binary (similar to an ultraluminous X-ray source; ULX) might correspond to the PRS of the FRB. In this scenario, there should be a persistent X-ray counterpart to account for the ULX origin. Many of the radio properties of the PRS of the FRB 20190520B are consistent with the hyper-accretion binary scenario, particularly when the apparent radio variability (Zhang et al. 2023) is attributed to scintillation (Bhandari et al. 2023a). Recently, off-nuclear compact radio sources have been detected in some dwarf galaxies (Reines et al. 2020), likely powered by an accreting intermediate-mass black hole (IMBH, 10^3 – $10^6 M_\odot$). These sources exhibit many similarities to the two FRB PRSs, including their radio luminosity, spectra and variability (Eftekhari et al. 2020; Law et al. 2022).

If the source behind the PRS is an accreting compact object, which may include but is not limited to hyper-accretion systems, we can compare our derived properties in the radio and X-ray band with those measurements taken from accreting black holes (BHs) and neutron stars. There is an established, empirical fundamental plane that characterizes accretion and jet activities of BHs, which demonstrates a universal correlation between X-ray luminosity, radio luminosity, and BH mass across a broad range of masses, encompassing both X-ray binaries (XRBs) and AGNs. We have re-plotted this fundamental plane using the data and best-fitting results from Gültekin et al. (2019). Additionally, we included some samples of the AGNs harboring IMBHs compiled by Yang & Yang (2023). Some of these samples show obvious deviations from the fundamental plane (Figure 3, see also Gültekin et al. 2022). The boosted radio emission and/or extended jet could cause such deviations (Yang & Yang 2023).

We also plotted some extragalactic ULXs (Laor & Behar 2008; Mezcua et al. 2015, 2018; Soria et al. 2021), which are thought to be IMBH candidates or super-Eddington accreting stellar-mass compact objects. For these ULXs, we plotted both $10 M_\odot$ BH mass and the mass estimations in the literature (or $1000 M_\odot$ if no mass estimate was available). The nature of the radio emission from ULXs is still under debate. Some are thought to originate from jet emission, which tends to be more radio-loud compared to emission from nebulae. High resolution VLBI observations of these sources can resolve the jet structures. For example, both a radio core and large-scale radio lobes have been detected in NGC 2276-3c (Mezcua et al. 2015). The radio core emission from this source aligns with the fundamental plane if the black hole mass is assumed to be approximately $5 \times 10^4 M_\odot$. Similarly, two radio lobes have also been observed in the ULX CXO J133815.6+043255 in NGC 5252. The total radio emission from both ULXs is believed to arise from extended jets rather than a compact core jet.

Since the position of the PRS of FRB 20190520B is off-nuclear (Niu et al. 2022), its radio emission can not be attributed to the activity of the central super-massive or intermediate-mass BH in the dwarf galaxy. If the PRS is powered by an accreting BH, the BH mass is likely less than $10^6 M_\odot$, as inferred from the fundamental plane (see also Zhang et al. 2023). So we plotted a vertical line below $10^6 M_\odot$ as the lower limit of the PRS of FRB 20190520B in the diagram of Figure 3. We also display the lower limits corresponding to different compact object masses: 1.4, 10, 10^3 and $10^5 M_\odot$.

Eftekhari et al. (2023) have given a more stringent upper limit of 6.57×10^{41} erg s $^{-1}$ based on a 14.9 ks *Chandra* observation. The lower limit range calculated from this constraint is also plotted as a vertical dash-dotted line in black. The lower limit range corresponding to the first detected PRS associated with FRB 20121102A is also plotted (Chatterjee et al. 2017; Eftekhari et al. 2023).

FRB 20201124A is the third FRB found associated with a PRS (Bruni et al. 2024; Dong et al. 2024). However the size of its reported PRS is significantly more extended than the other two (Chatterjee et al. 2017; Bhandari et al. 2023b; Bruni et al. 2024), which suggests that it might be a PRS with significant differences from the two more compact PRSs. We used the reported flux of the compact radio emission (Bruni et al. 2024) and the X-ray upper limit (Piro et al. 2021) to calculate the lower limit range. The three PRSs all reside in the lower right region below the fundamental plane of the accreting BHs in Figure 3.

To illustrate additional representative systems that have been considered as potential candidates for PRSs, we have included the data from the Crab nebula (Lyutikov et al. 2019), an extragalactic SNR (Mezcua et al. 2013), and a nebula of the Galactic XRB SS 433 (Wolter et al. 2015). Obviously, these sources do not follow the fundamental plane, since their radio emission is not powered by compact jets as in accreting black hole systems.

We summarize the insights from the diagram of Figure 3. The PRS of FRB 20190520B is more radio-loud than the brightest SNR, Crab nebula, SS433 and several ULXs. Notably, the two ULXs with extended radio jets (namely CXO J133815.6+043255 and NGC 2276-3c) and a few AGNs harboring IMBHs are positioned close to the lower limit of the three FRBs (see Figure 3). The radio spectral index of the PRS of FRB 20190520B is -0.40 ± 0.06 (Zhang et al. 2023), which is also similar to the extended jet of the two ULXs (-0.5 ± 0.2 for NGC 2276-3c and -0.66 ± 0.02 for CXO J133815.6+043255; Mezcua et al. 2015; Smith et al. 2023). However, the radio luminosity of the PRS of FRB 20190520B ($\sim 10^{39}$ erg s $^{-1}$) is roughly two orders of magnitude larger than that of the radio jets of the two ULXs ($\sim 10^{37}$ erg s $^{-1}$). This suggests that the PRS of FRB 20190520B must either possess a substantially more luminous extended radio jet or the observed radio jet emission is significantly beamed and boosted if corresponding source is a ULX of a similar type, as discussed for a potential PRS origin of accreting compact objects with an uncertain range of masses (Zhang et al. 2023). It is worth noting that the rare association of FRBs with a PRS within the entire FRB population (only a few cases out of a thousand or more FRBs), can be straightforwardly explained if the radio emission of the PRS of FRB 20190520B is beamed in a small solid angle, on the order of $1/1000$ of 4π , and boosted by relativistic effects.

We would like to thank the anonymous referee for stimulating and helpful comments and suggestions. WY would like to thank the *Swift* PI, Brad Cenko (and his designate) for approving and scheduling our *Swift* observations. We appreciate the *Swift* team for helping with quick data access. We would like to thank the FAST TAC to approve our DDT observations and the FRB Key Science Project for the arrangement of half of the FAST observations that are reported in this paper. WY, ZY and DL would like to acknowledge support by the National Natural Science Foundation of China (grant number 11333005, U1838203, U1938114, 11988101, 12361131579, 12373049 and 12373050). ZY was also supported in part by the Youth Innovation Promotion Association of Chinese Academy of Sciences. DL is a New Cornerstone Investigator. KLP acknowledges funding from the UK Space Agency.

Facilities: Swift, FAST

Software: astropy (Astropy Collaboration et al. 2018), matplotlib, proplot(Davis 2021),HEASoft

REFERENCES

- Anna-Thomas, R., Connor, L., Dai, S., et al. 2023, Science, 380, 599, doi: [10.1126/science.abo6526](https://doi.org/10.1126/science.abo6526)
- Astropy Collaboration, Price-Whelan, A. M., Sipőcz, B. M., et al. 2018, AJ, 156, 123, doi: [10.3847/1538-3881/aabc4f](https://doi.org/10.3847/1538-3881/aabc4f)
- Bassa, C. G., Tendulkar, S. P., Adams, E. A. K., et al. 2017, ApJL, 843, L8, doi: [10.3847/2041-8213/aa7a0c](https://doi.org/10.3847/2041-8213/aa7a0c)
- Beloborodov, A. M. 2020, ApJ, 896, 142, doi: [10.3847/1538-4357/ab83eb](https://doi.org/10.3847/1538-4357/ab83eb)
- Bhandari, S., Marcote, B., Sridhar, N., et al. 2023a, ApJL, 958, L19, doi: [10.3847/2041-8213/ad083f](https://doi.org/10.3847/2041-8213/ad083f)
- . 2023b, ApJL, 958, L19, doi: [10.3847/2041-8213/ad083f](https://doi.org/10.3847/2041-8213/ad083f)
- Bochenek, C. D., Ravi, V., Belov, K. V., et al. 2020, Nature, 587, 59, doi: [10.1038/s41586-020-2872-x](https://doi.org/10.1038/s41586-020-2872-x)
- Bruni, G., Piro, L., Yang, Y.-P., et al. 2024, Nature, 632, 1014, doi: [10.1038/s41586-024-07782-6](https://doi.org/10.1038/s41586-024-07782-6)
- Chatterjee, S., Law, C. J., Wharton, R. S., et al. 2017, Nature, 541, 58, doi: [10.1038/nature20797](https://doi.org/10.1038/nature20797)
- Chen, G., Ravi, V., & Hallinan, G. W. 2023, ApJ, 958, 185, doi: [10.3847/1538-4357/ad02f3](https://doi.org/10.3847/1538-4357/ad02f3)
- Chen, G., Ravi, V., & Lu, W. 2020, The Astrophysical Journal, 897, 146, doi: [10.3847/1538-4357/ab982b](https://doi.org/10.3847/1538-4357/ab982b)
- Chen, H.-Y., Gu, W.-M., Fu, J.-B., et al. 2022, ApJ, 937, 9, doi: [10.3847/1538-4357/ac8b7f](https://doi.org/10.3847/1538-4357/ac8b7f)
- Davis, L. L. B. 2021, ProPlot, v0.9.5, Zenodo, doi: [10.5281/zenodo.5602155](https://doi.org/10.5281/zenodo.5602155)
- Dong, Y., Eftekhari, T., Fong, W.-f., et al. 2024, ApJ, 961, 44, doi: [10.3847/1538-4357/ad0cbd](https://doi.org/10.3847/1538-4357/ad0cbd)
- Eftekhari, T., Berger, E., Margalit, B., Metzger, B. D., & Williams, P. K. G. 2020, ApJ, 895, 98, doi: [10.3847/1538-4357/ab9015](https://doi.org/10.3847/1538-4357/ab9015)
- Eftekhari, T., Fong, W., Gordon, A. C., et al. 2023, arXiv e-prints, arXiv:2307.03766, doi: [10.48550/arXiv.2307.03766](https://doi.org/10.48550/arXiv.2307.03766)
- Evans, P. A., Beardmore, A. P., Page, K. L., et al. 2007, A&A, 469, 379, doi: [10.1051/0004-6361:20077530](https://doi.org/10.1051/0004-6361:20077530)
- Gehrels, N., Chincarini, G., Giommi, P., et al. 2004, ApJ, 611, 1005, doi: [10.1086/422091](https://doi.org/10.1086/422091)
- Guidorzi, C., Marongiu, M., Martone, R., et al. 2020a, A&A, 637, A69, doi: [10.1051/0004-6361/202037797](https://doi.org/10.1051/0004-6361/202037797)
- Guidorzi, C., Orlandini, M., Frontera, F., et al. 2020b, A&A, 642, A160, doi: [10.1051/0004-6361/202039129](https://doi.org/10.1051/0004-6361/202039129)
- Gültekin, K., King, A. L., Cackett, E. M., et al. 2019, ApJ, 871, 80, doi: [10.3847/1538-4357/aaf6b9](https://doi.org/10.3847/1538-4357/aaf6b9)
- Gültekin, K., Nyland, K., Gray, N., et al. 2022, MNRAS, 516, 6123, doi: [10.1093/mnras/stac2608](https://doi.org/10.1093/mnras/stac2608)
- He, C., Ng, C. Y., & Kaspi, V. M. 2013, ApJ, 768, 64, doi: [10.1088/0004-637X/768/1/64](https://doi.org/10.1088/0004-637X/768/1/64)
- Hiramatsu, D., Berger, E., Metzger, B. D., et al. 2023, ApJL, 947, L28, doi: [10.3847/2041-8213/aca9e8](https://doi.org/10.3847/2041-8213/aca9e8)
- Kilpatrick, C. D., Tejos, N., Andersen, B. C., et al. 2024, ApJ, 964, 121, doi: [10.3847/1538-4357/ad2687](https://doi.org/10.3847/1538-4357/ad2687)
- Kumar, P., Lu, W., & Bhattacharya, M. 2017, MNRAS, 468, 2726, doi: [10.1093/mnras/stx665](https://doi.org/10.1093/mnras/stx665)
- Laha, S., Younes, G., Wadiasingh, Z., et al. 2022, The Astrophysical Journal, 930, 172, doi: [10.3847/1538-4357/ac63a8](https://doi.org/10.3847/1538-4357/ac63a8)
- Laor, A., & Behar, E. 2008, MNRAS, 390, 847, doi: [10.1111/j.1365-2966.2008.13806.x](https://doi.org/10.1111/j.1365-2966.2008.13806.x)
- Law, C. J., Connor, L., & Aggarwal, K. 2022, ApJ, 927, 55, doi: [10.3847/1538-4357/ac4c42](https://doi.org/10.3847/1538-4357/ac4c42)
- Lee, K.-G., Khrykin, I. S., Simha, S., et al. 2023, ApJL, 954, L7, doi: [10.3847/2041-8213/acefb5](https://doi.org/10.3847/2041-8213/acefb5)
- Li, D., Dickey, J. M., & Liu, S. 2019, Research in Astronomy and Astrophysics, 19, 016, doi: [10.1088/1674-4527/19/2/16](https://doi.org/10.1088/1674-4527/19/2/16)
- Li, D., Wang, P., Qian, L., et al. 2018, IEEE Microwave Magazine, 19, 112, doi: [10.1109/MMM.2018.2802178](https://doi.org/10.1109/MMM.2018.2802178)
- Li, D., Wang, P., Zhu, W. W., et al. 2021, Nature, 598, 267, doi: [10.1038/s41586-021-03878-5](https://doi.org/10.1038/s41586-021-03878-5)
- Lu, W., Kumar, P., & Zhang, B. 2020, MNRAS, 498, 1397, doi: [10.1093/mnras/staa2450](https://doi.org/10.1093/mnras/staa2450)
- Lyubarsky, Y. 2014, MNRAS, 442, L9, doi: [10.1093/mnras/flu046](https://doi.org/10.1093/mnras/flu046)

- Lyutikov, M., Temim, T., Komissarov, S., et al. 2019, *MNRAS*, 489, 2403, doi: [10.1093/mnras/stz2023](https://doi.org/10.1093/mnras/stz2023)
- Metzger, B. D., Margalit, B., & Sironi, L. 2019, *MNRAS*, 485, 4091, doi: [10.1093/mnras/stz700](https://doi.org/10.1093/mnras/stz700)
- Mezcua, M., Kim, M., Ho, L. C., & Lonsdale, C. J. 2018, *MNRAS*, 480, L74, doi: [10.1093/mnrasl/sly130](https://doi.org/10.1093/mnrasl/sly130)
- Mezcua, M., Lobanov, A. P., & Martí-Vidal, I. 2013, *MNRAS*, 436, 2454, doi: [10.1093/mnras/stt1738](https://doi.org/10.1093/mnras/stt1738)
- Mezcua, M., Roberts, T. P., Lobanov, A. P., & Sutton, A. D. 2015, *MNRAS*, 448, 1893, doi: [10.1093/mnras/stv143](https://doi.org/10.1093/mnras/stv143)
- Michilli, D., Seymour, A., Hessels, J. W. T., et al. 2018, *Nature*, 553, 182, doi: [10.1038/nature25149](https://doi.org/10.1038/nature25149)
- Nan, R., Li, D., Jin, C., et al. 2011, *International Journal of Modern Physics D*, 20, 989, doi: [10.1142/S0218271811019335](https://doi.org/10.1142/S0218271811019335)
- Nicastro, L., Guidorzi, C., Palazzi, E., et al. 2021, *Universe*, 7, 76, doi: [10.3390/universe7030076](https://doi.org/10.3390/universe7030076)
- Niu, C. H., Aggarwal, K., Li, D., et al. 2022, *Nature*, 606, 873, doi: [10.1038/s41586-022-04755-5](https://doi.org/10.1038/s41586-022-04755-5)
- Oates, S. R., Page, M. J., Schady, P., et al. 2009, *MNRAS*, 395, 490, doi: [10.1111/j.1365-2966.2009.14544.x](https://doi.org/10.1111/j.1365-2966.2009.14544.x)
- Pilia, M., Burgay, M., Possenti, A., et al. 2020, *ApJL*, 896, L40, doi: [10.3847/2041-8213/ab96c0](https://doi.org/10.3847/2041-8213/ab96c0)
- Piro, L., Bruni, G., Troja, E., et al. 2021, *A&A*, 656, L15, doi: [10.1051/0004-6361/202141903](https://doi.org/10.1051/0004-6361/202141903)
- Principe, G., Di Venere, L., Negro, M., et al. 2023, *A&A*, 675, A99, doi: [10.1051/0004-6361/202346492](https://doi.org/10.1051/0004-6361/202346492)
- Rajwade, K. M., Mickaliger, M. B., Stappers, B. W., et al. 2020, *MNRAS*, 495, 3551, doi: [10.1093/mnras/staa1237](https://doi.org/10.1093/mnras/staa1237)
- Reines, A. E., Condon, J. J., Darling, J., & Greene, J. E. 2020, *ApJ*, 888, 36, doi: [10.3847/1538-4357/ab4999](https://doi.org/10.3847/1538-4357/ab4999)
- Rhodes, L., Caleb, M., Stappers, B. W., et al. 2023, *MNRAS*, 525, 3626, doi: [10.1093/mnras/stad2438](https://doi.org/10.1093/mnras/stad2438)
- Scholz, P., Bogdanov, S., Hessels, J. W. T., et al. 2017, *ApJ*, 846, 80, doi: [10.3847/1538-4357/aa8456](https://doi.org/10.3847/1538-4357/aa8456)
- Sironi, L., Plotnikov, I., Nättilä, J., & Beloborodov, A. M. 2021, *PhRvL*, 127, 035101, doi: [10.1103/PhysRevLett.127.035101](https://doi.org/10.1103/PhysRevLett.127.035101)
- Smith, K. L., Magno, M., & Tripathi, A. 2023, *ApJ*, 956, 3, doi: [10.3847/1538-4357/acf4f8](https://doi.org/10.3847/1538-4357/acf4f8)
- Soria, R., Pakull, M. W., Motch, C., et al. 2021, *MNRAS*, 501, 1644, doi: [10.1093/mnras/staa3784](https://doi.org/10.1093/mnras/staa3784)
- Sridhar, N., & Metzger, B. D. 2022, *ApJ*, 937, 5, doi: [10.3847/1538-4357/ac8a4a](https://doi.org/10.3847/1538-4357/ac8a4a)
- Sun, S., Yu, W., Yu, Y., Mao, D., & Lin, J. 2019, *The Astrophysical Journal*, 885, 55, doi: [10.3847/1538-4357/ab4420](https://doi.org/10.3847/1538-4357/ab4420)
- Tavani, M., Verrecchia, F., Casentini, C., et al. 2020, *ApJL*, 893, L42, doi: [10.3847/2041-8213/ab86b1](https://doi.org/10.3847/2041-8213/ab86b1)
- Tendulkar, S. P., Bassa, C. G., Cordes, J. M., et al. 2017, *The Astrophysical Journal*, 834, L7, doi: [10.3847/2041-8213/834/2/L7](https://doi.org/10.3847/2041-8213/834/2/L7)
- Trudu, M., Pilia, M., Nicastro, L., et al. 2023, *A&A*, 676, A17, doi: [10.1051/0004-6361/202245303](https://doi.org/10.1051/0004-6361/202245303)
- Wolter, A., Rushton, A., Mezcua, M., et al. 2015, in *Advancing Astrophysics with the Square Kilometre Array (AASKA14)*, 91, doi: [10.22323/1.215.0091](https://doi.org/10.22323/1.215.0091)
- Yang, X., & Yang, J. 2023, *Galaxies*, 11, 53, doi: [10.3390/galaxies11020053](https://doi.org/10.3390/galaxies11020053)
- Yang, Y.-P., & Zhang, B. 2018, *ApJ*, 868, 31, doi: [10.3847/1538-4357/aae685](https://doi.org/10.3847/1538-4357/aae685)
- Zhang, B. 2020, *Nature*, 587, 45, doi: [10.1038/s41586-020-2828-1](https://doi.org/10.1038/s41586-020-2828-1)
- . 2023, *Reviews of Modern Physics*, 95, 035005, doi: [10.1103/RevModPhys.95.035005](https://doi.org/10.1103/RevModPhys.95.035005)
- Zhang, X., Yu, W., Law, C., et al. 2023, *ApJ*, 959, 89, doi: [10.3847/1538-4357/ad0545](https://doi.org/10.3847/1538-4357/ad0545)

Table 2. The observations of *Swift*/BAT for the event data analysis

obsID	start time (UTC)	exposure (seconds)
00968731000	2020-04-30 12:53:02	120
00972010000	2020-05-13 13:23:32	272
00972011000	2020-05-13 13:33:27	1023
00972030000	2020-05-13 14:51:48	1142
00973140000	2020-05-19 11:16:44	1202
00088915014	2020-05-20 14:10:19	200
00973140006	2020-05-22 15:36:09	200
00974942000	2020-05-29 00:52:56	1122
00975895000	2020-06-03 19:25:16	1202
00089076001	2020-07-14 05:55:33	121
00095656005	2020-07-18 08:24:09	200
00013597029	2020-08-23 11:13:08	200
00095660154	2020-09-16 06:01:40	200
00996184000	2020-09-17 03:48:49	1202
00996184003	2020-09-19 14:58:12	200

Table 3. The properties of the detected FRB bursts during the *Swift* observations.

Burst time ^a (MJD)	DM (pc cm ⁻³)	Pulse width (ms)	Energy ($\times 10^{37}$ erg)	XRT time (MJD)	U time (MJD)
58991.7289360891	1214.2	30.2	16.8	58991.728923501	...
59067.484346541	1202.8	14.9	15.9	59067.484320859	59067.484320927
59067.4843471197	1202.8	33.1	17.8	59067.484320859	59067.484321482
59071.470504066	1200.0	5.2	9.6	59071.470485296	59071.470478477
59071.4705042975	1200.0	7.2	8.1	59071.470485296	59071.470478755
59075.4527133255	1210.6	24.9	38.0	59075.452698807	59075.452687499
59075.453222841	1210.6	22.0	25.5	59075.453192673	59075.453196944
59077.496363178	1218.6	15.3	16.8	59077.496344162	59077.496337235
59077.4965143868	1218.6	13.6	10.9	59077.496489417	59077.496488346
59077.497517645	1218.6	4.6	11.4	59077.497477148	59077.497491680

^a The burst time is at Coordinated Universal Time (UTC), which is referenced to 1.5 GHz.

APPENDIX